


Received July 25, 2019, accepted August 12, 2019, date of publication August 19, 2019, date of current version September 6, 2019.

Digital Object Identifier 10.1109/ACCESS.2019.2936306

# Analytical Design Procedure for Forward Wave Couplers in RGW Technology Based on Hybrid PEC/PMC Waveguide Model

**ABDULADEEM BELTAYIB** , (Student Member, IEEE), AND

**ABDEL-RAZIK SEBAK** , (Life Fellow, IEEE)

Electrical and Computer Engineering Department, Concordia University, Montreal, QC H4B 1R6, Canada

Corresponding author: Abduladeem Beltayib (A\_beltay@encs.concordia.ca)

**ABSTRACT** In this paper, a systematic design methodology of a 0dB and a 3dB forward couplers based on the ridge gap waveguide (RGW) technology is presented. This methodology is based on exact theoretical formulations rather than any approximate or empirical equations. The procedure of the proposed design methodology is mainly to build a virtual equivalent waveguide model. This waveguide has two horizontal upper and lower perfect electric conductor (PEC) walls, while the left and the right walls are made of perfect magnetic conductors (PMC). A detailed analysis for this hybrid PEC/PMC waveguide, a common waveguide for coupling, is introduced as the starting phase for designing the RGW couplers. The equivalent RGW coupler that assures the same operation of the hybrid PEC/PMC waveguide at a specific frequency range is deduced based on detailed theoretical aspects. Moreover, a simple analyzing of transitional bends and phase shifters with accurate calculations is presented in this paper, which are the fundamental building blocks of several mmW components such as the six-port junction and the butler matrix. The possibility of tuning the coupler center frequency is introduced without the need of using any nonlinear elements. The resulting RGW couplers are implemented through well-known full wave simulator (Ansoft HFSS), with verification through prototype measurements in order to confirm the validity of the proposed methodology. A good agreement is achieved between measurement and simulation results.

**INDEX TERMS** Hybrid forward couplers, periodic structure, ridge gap waveguide, hybrid PEC/PMC waveguide.

## I. INTRODUCTION

Forward wave couplers are essential elements in microwave circuits and wireless communication systems. They play an important role in splitting the power among different devices. Such power splitters can be classified as couplers or hybrid junctions [1]. Many previous research efforts are conducted for implementing forward wave couplers based on different technologies. Some couplers are based on rectangular waveguides (RWG) [2], microstrip lines [3], substrate integrated waveguide (SIW) [4], nonradiative dielectric (NRD) waveguide [5], [6] and ridge gap waveguide (RGW) [7]–[9].

Unfortunately, most of the mentioned technologies have some limitations that could negatively affect the hybrid junction operation. For example, the rectangular

waveguide is bulky and hard to be integrated with other waveguides at high frequencies in particular at millimeter wave (mmW) band. Moreover, either the microstrip or the SIW technologies introduce high dielectric losses at high frequencies. The previously-mentioned problems make the study of the RGW technology for designing microwave components with better performance is preferred.

The RGW technology provides solutions for the mentioned problems that occur in other technologies. First, the RGW eliminates dielectric losses because the wave propagates in an air-gap between the ridge and the upper plate. Second, the RGW can be designed in a printed form which makes it integrable with other circuits. Based on the mentioned advantages of the RGW, it should be considered as a promising candidate for high frequency applications, especially for the fifth generation (5G) applications of wireless technology [10].

The associate editor coordinating the review of this article and approving it for publication was Yongle Wu.

Moreover, RGW technology is an important candidate for the implementation of slot array antennas [11]–[13].

The basic models for the periodic unit cells of the RGW is reported in [14]–[16]. Most of the existing research about microwave components based on RGW technology mainly depend on approximate or empirical equations [7], [17]. In [18], PEC-over-PMC ideal ridge gap waveguide is applied. This model consists of a strip line in a homogenous medium. The periodic structure is considered as a horizontal surface of a PMC. This model represents a good approximation which reduces the time consumption on the full-wave simulators. However, it still needs optimization on the realized structure. This could complicate the generalized design procedure for such microwave components. Therefore, it is extremely important to have a clear theoretical design procedure for the RGW-based applications. In [19], the expression for the electric field component on the ridge is written based on the PMC boundary conditions is presented, which consider a good and simple approximation.

In this paper, an analytical design procedure of forward wave couplers based on RGW technology is introduced. This procedure is mainly based on a hybrid PEC/PMC waveguide. This hybrid waveguide represents an ideal RGW where the periodic sides of the RGW, the two bed-of-nails and their cover are replaced with a vertical (rather than horizontal as usually represented) PMC boundary. This is in addition to the upper and lower PEC boundaries. The analysis of this hybrid waveguide is as simple as the analysis of rectangular waveguides but with some differences explained in details in this paper. This analysis is then used as the starting phase in designing the RGW hybrid junction. In order for the RGW to operate exactly as the hybrid PEC/PMC waveguide, the periodic bed of nails should be modeled to behave as a vertical PMC wall.

Furthermore, this hybrid waveguide facilitates analyzing even the transitional bends and phase shifters with accurate calculations which are the main building blocks of many mmW components such as the six-port junction and the butler matrix.

The design procedure of the RGW-based hybrid junction starts by deriving the field solutions and dispersion equations of the hybrid PEC/PMC waveguide. The obtained dispersion is used for calculating the required coupling length at the operating frequency range. The coupling mechanism in this case is based on Riblet (short slot) coupler [20]. The next step is to implement the RGW coupler based on the dimensions obtained from the hybrid PEC/PMC waveguide. A comparison between the results of the hybrid PEC/PMC waveguide coupler and the RGW-based coupler leads to an important observation. This comparison confirms that the RGW width is not constant with frequency which may be considered as an effective width that varies with frequency. In other words, the equivalence between the hybrid PEC/PMC waveguide width and the RGW effective width is a frequency-dependent property. This is explained in details through the paper sections.

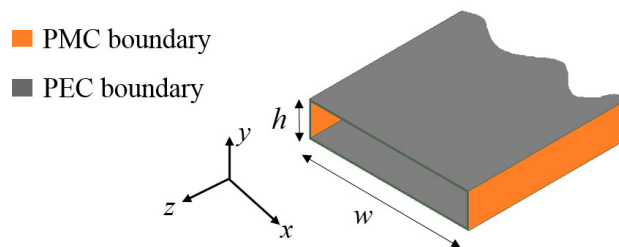


FIGURE 1. Equivalent hybrid PEC/PMC waveguide.

Recent research about microwave components based on RGW technology mainly depends on approximate or empirical equations. For example and to the best of our knowledge, there is no reported work in the literature uses even and odd mode to obtain coupling length of this type of forward coupler. Thus, the long processing time for optimization is needed. This complicates the design procedure for such microwave components. Therefore, it is extremely important to have a clear and simple theoretical design procedure for the RGW-based components. In this work, a simple model represents a good approximation of the RGW based on theoretical analysis is introduced, which reduces the computational time of full-wave simulators.

The paper is organized as follows, in Sec. II, the operation of the proposed hybrid PEC/PMC waveguide model is introduced. In Sec. III, a hybrid junction based on the hybrid PEC/PMC waveguide is analyzed and designed. Then, the analytical analysis and design methodology of the RGW coupler is discussed in Sec. IV. In this section, the unit cell design is presented, then the dispersion of RGW and the excitation of the RGW through a circulating bend is shown. Accordingly, the full coupler design with the tunability mechanism are depicted. After that in Sec. V, a possible setup for a physical realization of the RGW coupler is discussed. Finally, conclusions are given in Sec. VI.

## II. HYBRID PEC/PMC WAVEGUIDE OPERATION

The main objective of this section is to develop the concept of a factitious type of waveguides referred to as the hybrid PEC/PMC waveguide. This is to facilitate and simplify the theoretical analysis which would be rather complicated if the RGW is analyzed directly in its complete form. In Fig. 1, an equivalent hybrid PEC/PMC waveguide is presented. The operation of the hybrid PEC/PMC waveguide is introduced firstly in this section. Then later in section IV, the relation between this hybrid PEC/PMC waveguide and the realistic ridge gap waveguide is explained.

The waveguide in Fig. 1 consists of two vertical PMC walls and two horizontal PEC walls. For simplicity and without loss of generality, the waveguide is assumed to be filled with free space. The waveguide width is  $w$  while its height is  $h$ . It is assumed that  $h$  is always much smaller than  $w$ . Accordingly, only the modes that are uniform in the vertical  $y$ -direction are the modes of interest in this paper.

To find full expressions for the field of those modes, one can follow a traditional solution methodology to solve the Heaviside wave equation in rectangular coordinates [21]. The solution of the wave equation has to satisfy special boundary conditions. That is tangential electric field has to vanish on the top and bottom PEC walls, while the tangential magnetic field has to vanish on the left and right PMC walls. This later condition is different from the traditional boundary condition known in conventional rectangular PEC waveguides.

In order to satisfy this special boundary condition at PMC walls, one can write the expression for the tangential electric field component as follows,

$$E_y = \sum_{m=0,2,4}^{\infty} E_m \cos(\beta_{xm}x) e^{-j\beta_{zm}z} + \sum_{m=1,3,5}^{\infty} E_m \sin(\beta_{xm}x) e^{-j\beta_{zm}z}. \quad (1)$$

where  $x = 0$  is taken at the center of the waveguide,  $\beta_{zm}$  is the propagation constant in  $z$ -direction and  $\beta_{xm}$  is the propagation constant in  $x$ -direction which can be written as,

$$\beta_{xm} = \frac{m\pi}{w}, \quad m = 0, 1, 2, 3. \quad (2)$$

The relation between  $\beta_{zm}$  and  $\beta_{xm}$  is given by

$$\beta_{zm}^2 + \beta_{xm}^2 = k_0^2 = \omega^2 \mu_0 \epsilon_0. \quad (3)$$

where  $k_0$  is the wavenumber,  $\omega = 2\pi f$  is the radial frequency,  $\mu_0, \epsilon_0$  are the permeability and permittivity of free space, respectively.

The mode which corresponds to  $m = 0$  is the well-known TEM parallel plate mode with propagation only in the  $z$ -direction and uniform distribution in the  $x$ - and  $y$ -directions. This mode has real propagation constant in the  $z$ -direction  $\beta_{zm}$  for all frequencies down to DC, regardless of the width  $w$ , as shown by the solid blue curve in Fig. 2a. Furthermore, this propagation constant is equal to the wavenumber in free space,  $k_0$ . The electric field  $E_y$  of this mode as a function of  $x$  is shown by the solid blue curve in Fig. 2b.

Assuming the vertical PMC walls are not factitious and can be truly realized with certain artificial material, we consider the behavior of the first higher order mode corresponding to  $m = 1$  as a plane wave propagating back and forth between the two PMC walls. The reflection coefficient of the those walls must be in the way that cancels out the tangential magnetic field components and not the electric field components as in the conventional PEC waveguide, i.e., the reflection coefficient magnitude has to be equal to unity.

Consequently, the wave will be guided in the region between those two factitious PMC walls with the tangential electric field taking maximum value at PMC walls. The propagation constant of this mode in  $z$ -direction is purely imaginary below certain frequency which is determined by the distance between the two PMC walls,  $w$ . That is,

$$\beta_{z1} = \sqrt{k_0^2 - \left(\frac{\pi}{w}\right)^2}. \quad (4)$$

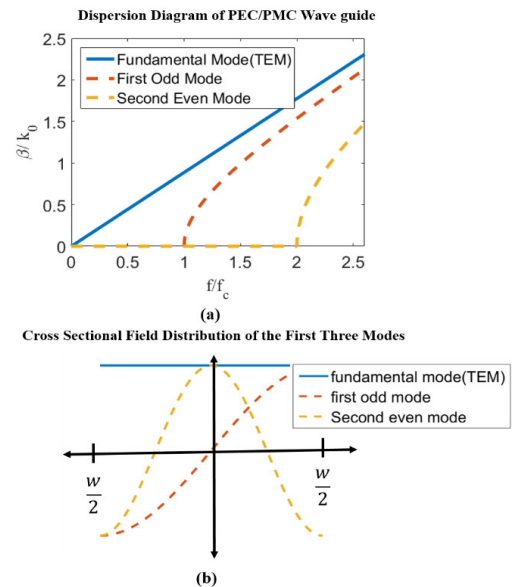


**FIGURE 2. Hybrid PEC/PMC waveguide: (a) dispersion curves, (b) cross-sectional electric field distribution for the TEM, TE10 and TE20 modes, respectively at  $w_r = 13$  mm.**

From (4), one can deduce that  $\beta_{z1}$  is pure imaginary for all frequencies below  $f_{c\_PMC/PEC} = c/2w$ . The behavior of the real part of  $\beta_{z1}$  is shown versus frequency by the dashed red curve of Fig. 2a, while the electric field  $E_y$  of this mode as a function of  $x$  is shown by the dashed red curve in Fig. 2b.

Although this mode is the first higher order mode and not the dominant mode, it resembles in behavior the dominant mode of a conventional PEC waveguide except that the electric field is maximum at the PMC walls and zero at the center, i.e. it has an odd symmetry about the longitudinal axis of the guide. The next higher order mode will be of even symmetry and has a cutoff frequency which is double that of the first higher order mode, as shown in Fig. 2. As a further illustration, assume  $w = 5$  mm and  $h = 1$  mm. The fundamental propagating mode is the TEM mode with  $m = 0$  for all frequencies. The cutoff of the first higher order mode is  $f_{c\_PMC/PEC} = c/2w = 30$  GHz. Therefore, at 13 GHz for example, the field distribution will be as shown in Fig. 3a, where the only propagating mode is the uniform parallel plate mode, while the first higher order mode still cannot propagate.

For this mode to propagate, either the frequency of operation should be increased to be higher than 30 GHz or the width  $w$  should be increased such that  $f_{c\_PMC/PEC}$  is below 13 GHz. For example, if  $w = 13$  mm, the field distribution for the possible two modes at 13 GHz is shown in Fig. 3b. These deduced information can be used as the starting phase for designing a factitious forward wave coupler as explained in the following section.

### III. HYBRIDS PEC/PMC COUPLER

In general, the hybrid coupler is a kind of four ports directional coupler which can be designed to achieve theoretical coupling levels as high as 0dB. The coupling phenomenon

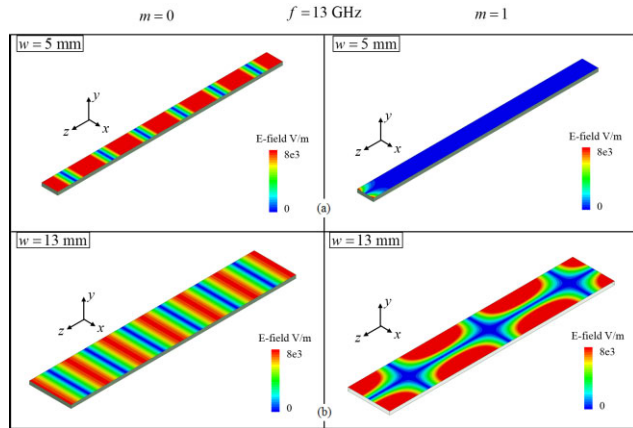


**FIGURE 3.** Field Distribution of the ideal PMC waveguide (a) at width  $w = 5 \text{ mm}$  of for  $m = 0$  and  $m = 1$  and (b) at  $w = 13 \text{ mm}$  for  $m = 0$  and  $m = 1$ .

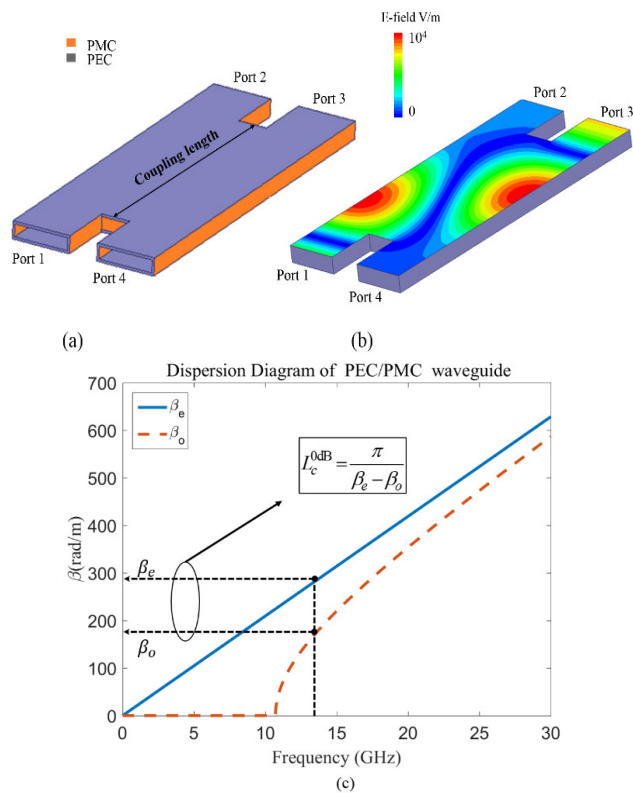


**FIGURE 4.** Hybrid PEC/PMC Coupler, (a) geometry, (b) electric field distribution at 13GHz and (c) dispersion diagram of the common section.

discussed in this section is mainly based on the concept of the Riblet coupler [20]. The Riblet coupler consists of two rectangular waveguides placed parallel to each other. The common wall is the short wall and this wall is totally opened between the guides for a certain coupling length, hence the name “short-slot” coupler.

The main goal in this section is to develop the concept of an artificial type of hybrid coupler based on the same concept of the Riblet coupler. We call this new type “Hybrid PEC/PMC” coupler. The configuration of the hybrid PEC/PMC coupler is shown in Fig.4a, where all the

vertical “short” walls are PMCs and the horizontal walls are PECs.

The structure consists of two Hybrid PEC/PMC waveguides parallel to each other. The common wall is the short PMC wall and this wall is totally opened between the guides for a certain coupling length. The required coupling level is achieved based on this specific coupling length  $l_c$ . The coupling length depends on the propagation constants of the even and odd order modes in the common section between the two waveguides. Those propagation constants can be determined from the discussion presented in Sec. II.

Ideally, the power fed to the structure from port1 is divided between ports 2 and 3 with no reflection at port1 and full isolation at port 4 [22]. The scattering parameters and power division between port2 and port3 can be formulated as [22].

$$S_{31} = \frac{e^{-j\beta_e l} - e^{-j\beta_o l}}{2} = -je^{-\frac{j(\beta_e + \beta_o)l}{2}} \sin\left[\left(\frac{\beta_e - \beta_o}{2}\right)l\right],$$

$$S_{21} = \frac{e^{-j\beta_e l} + e^{-j\beta_o l}}{2} = e^{-\frac{j(\beta_e + \beta_o)l}{2}} \cos\left[\left(\frac{\beta_e - \beta_o}{2}\right)l\right] \quad (5)$$

where  $S_{31}$  and  $S_{21}$  represent the transmission coefficients,  $\beta_e$  is the propagation constant of the first even (dominant) mode in the common section, i.e.  $\beta_e = \beta_{z0}$  defined in (2) and (3) for  $m = 0$ . Similarly,  $\beta_o$  is the propagation constant of the first odd mode in the common section, i.e.  $\beta_o = \beta_{z1}$ , defined also in (2) and (3) for  $m = 1$ . In (5),  $l$  denotes the length of the coupling section. Equation (5) shows that by obtaining the numerical value of the  $\beta_e$  and  $\beta_o$ , the required coupling length can be easily deduced without the need of empirical equations and optimizations. For example, if the input power should be completely transferred from port 1 to port 3, i.e. a coupling level of 0dB is required, then from (5), one can obtain the required coupling length according to,

$$S_{31} = 1 \implies l = l_c = \frac{\pi}{\beta_e - \beta_o} \quad (6)$$

The design procedure for the discussed artificial Hybrid PEC/PMC coupler is explained in the following example. Assume the operating frequency is selected to be 13 GHz. For proper operation of the coupler, the dimensions of the common section must be selected such that in this common area both the fundamental and the first higher order modes are excited. At the same time, the dimensions of the input ports must be selected to guarantee that only the fundamental mode is excited and no other mode can propagate.

As mentioned in Sec. II, the dominant mode has no cut-off while the cutoff frequency of the first odd mode is  $f_{c\_PMC/PEC} = c/2w$ , and the cutoff of the second higher order even mode is  $2f_{c\_PMC/PEC}$ . Thus, for only the first two modes to exist at the operating frequency, the width of the common section must satisfy

$$\frac{c}{2f_{c\_PMC/PEC}} < w < \frac{c}{f_{c\_PMC/PEC}} \quad (7)$$

At 13 GHz, the width can be chosen to be  $w = 13 \text{ mm}$ .



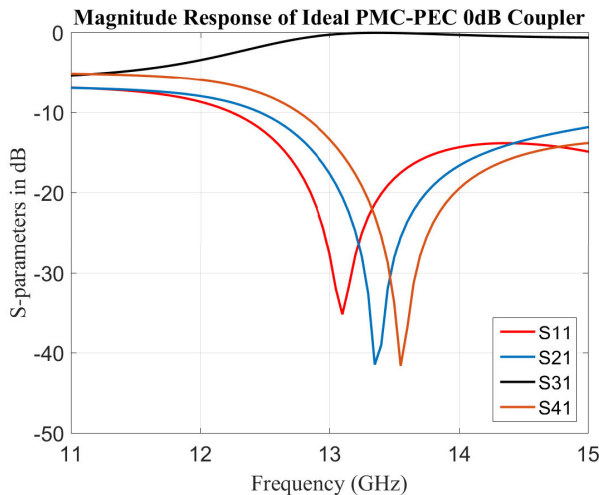


FIGURE 5. S-parameters of 0dB hybrid PEC/PMC waveguide coupler.

Physically, the width of the input waveguide must be less than half of the width of the common section. This should also guarantee that only the fundamental mode of each input waveguide can be excited. In this example, we take the width of the input ports to be  $w_r = 5\text{mm}$ . It is clear from the field distribution in Fig. 4b that the required design conditions are satisfied at the operating frequency of 13 GHz.

The last step of the design procedure is to determine the length of the common section which is the coupling length. To obtain the coupling length, one can substitute in (2) and (3) by  $w = 13\text{mm}$ ,  $m = 0$  to get  $\beta_e$  and by  $m = 1$  to get  $\beta_o$  at 13 GHz. Then substituting  $\beta_e$  and  $\beta_o$  in (6) gives the required coupling length, which is found to be 21 mm. The resultant dispersion curves are illustrated in Fig. 4c. With the obtained dimensions, full wave simulation gives the field distribution shown in Fig. 4b. The distribution shown confirms the occurrence of full coupling, where all the input power at port1 is transferred to port3 at the operating frequency.

The simulated S-parameters of the proposed hybrid PEC/PMC waveguide coupler is shown in Fig. 5 where the coupling level to port 3 is about 0dB from 13 to 15 GHz, the through level at port 2 and the isolation level at port 4 are below  $-15\text{dB}$ . Accordingly, it could be confirmed that the power is completely transferred from port1 to port 3 at the design frequency with a bandwidth behaviour governed by the dispersion curves shown in Fig. 4c.

Although the discussed coupler in this section is factitious, this design procedure is found to be very helpful to facilitate the design of realistic forward wave couplers based on modern technologies such as the ridge gap waveguide (RGW) technology. This is explained in the rest of this paper.

#### IV. ANALYTICAL DESIGN OF RGW COUPLER

Artificial magnetic conductors (AMC) have been an emerging topic of research in the past few years. AMC are made of periodic metallic structures. The geometry and the periodicity of those structures are designed in such a way that gives a

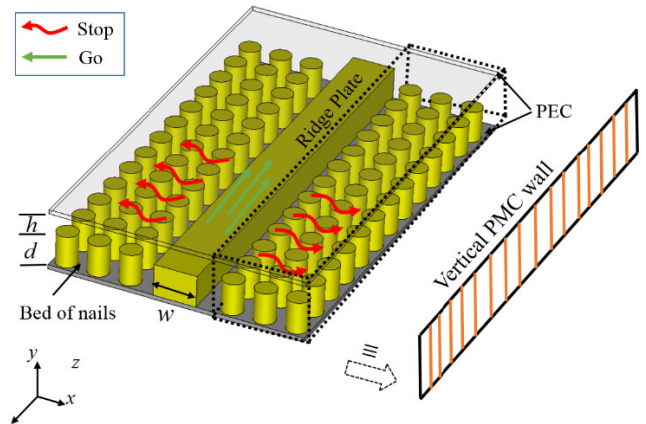


FIGURE 6. Complete Ridge Gap Waveguide configuration.

certain required behavior. The behavior of interest here is to design vertical guiding walls.

The RGW is a relatively new type of waveguides realized by the concept of the AMC. In this paper, RGW technology is modeled by the factitious hybrid-type of waveguides discussed in Sec. II.

The main objective of this section is to show the last step in the design procedure presented in Sec. III. That is the design of realistic forward wave couplers using the ridge gap waveguide technology. The obtained parameters from the hybrid PEC/PMC waveguide model can be used directly in the implementation of the region where the wave propagates (values of  $h$  and  $w$ ) in the realistic RGW.

Furthermore, the AMC in this design is realized by periodic perfect conducting cells. As shown in Fig.6, the vertical PMC boundaries model the whole dotted region enclosed by the top and bottom PEC plates containing the periodic cells. This is the novelty in this work whereas the dotted region was previously modeled as horizontal PMC boundary. This periodic part is used to block the electromagnetic waves from leaking outside the region on top of the ridge within certain stopband. This structure with such boundaries supports a quasi-TEM mode as the dominant mode.

In [14] the analytical solution of the dominant mode propagating through the RGW has been presented. In [14], the dispersion diagram was obtained theoretically and verified by full-wave eigenmode solver. This section focuses on summarizing the analytical solution presented in [14] to obtain the proper dimensions of the periodic part in order to act as perfect as the PMC boundary at the desired frequency band.

In addition to the solution provided in [14], we consider the first two modes not only the dominant mode. The study of the higher order modes gives the possibility of designing the RGW coupler analytically as shown in the following subsections.

##### A. DESIGN OF THE PERIODIC UNIT CELLS

The dispersion diagram of the unit cells is studied theoretically and then verified by using a commercial software (HFSS). The bed of nails configuration is shown in Fig. 7(a),

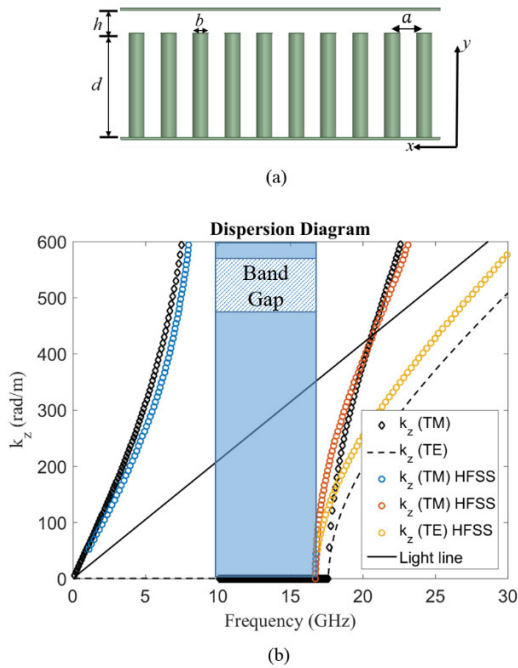


FIGURE 7. Periodic bed of nails, (a) geometry and (b) simulated and theoretical dispersion curves of the TE and TM modes.

where the cells are formed by metallic cylinders with radius  $b$ , height  $d$ , and with period  $a$ . The height of the nails  $d$  should be  $\lambda/4$  [14] and the total height between the two horizontal metal plates which is  $h + d$  equals  $\lambda/2$ , where  $h$  is the air gap between the bed of nails and the top plate, and  $\lambda$  is the free space wavelength. The characteristic impedance of AMC periodic structure depends on the dimensions of the unit cell. The TE and TM dispersion equations of this periodic structure can be formulated as in [14] where,

For the TE mode,

$$k_y = \frac{\pi}{(h + d)} \quad (8)$$

where  $k_y$  is the propagation constant in y-direction.

For the TM mode,

$$\frac{k_y}{k} \tan(k_y h) + \left[ 1 - \frac{k^2 - k_y^2}{k_p^2 + k^2 - k_y^2} \right] \tan(kd) + \frac{k^2 - k_y^2}{k_p^2 + k^2 - k_y^2} \frac{\sqrt{k_p^2 - k_y^2}}{k} \tan\left(\sqrt{k_p^2 - k_y^2} d\right) = 0 \quad (9)$$

where  $k_h = \sqrt{\epsilon_h} k$ ,  $\epsilon_h$  is the permittivity of host medium which is unity for simplicity,  $k$  is wavenumber and  $k_p$  is the plasma wavenumber where,

$$k_p = \frac{1}{a} \sqrt{\frac{2\pi}{\ln\left(\frac{a}{2\pi b}\right) + 0.5275}} \quad (10)$$

where this model is valid only when  $a/d, a/\lambda \ll 1$  as presented in [14]. The dispersion diagram in Fig. 7(b) gives

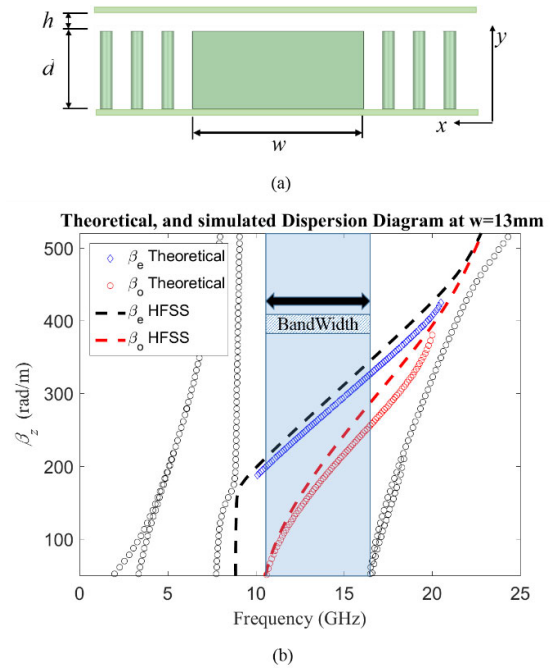


FIGURE 8. Comparison between dispersion curves of RGW obtained from HFSS and theoretically, at  $w = 13\text{mm}$ .

a clear illustration for showing the stop band of the periodic medium, where the dispersion relation is the relationship between the frequency and the propagation constant in  $z$  direction which can be written as

$$k_z = \sqrt{k^2 - k_y^2} \quad (11)$$

The unit cell dimensions is chosen to be the same as the dimensions presented in [14], where the height of the unit cell  $d = 7.5 \text{ mm}$ , radius  $b = 0.5 \text{ mm}$ , air gap is  $h = 1 \text{ mm}$  and the unit cells period  $a = 2 \text{ mm}$ . The dispersion curves with those dimensions of the periodic bed of nails is presented in Fig. 7(b) based on (8)-(11). The accuracy of the resulting dispersion equations are confirmed when compared with simulation results obtained from the HFSS eigenmode solver. Figure 7(b) shows that in the frequency range between 10 and 17GHz, there is no solution for (8) and (9) which gives real solution for (11). This means there is no propagating waves on the bed of nails within this band of frequencies. In this band, a wave incident from the middle region in Fig. 6 does not have the possibility of propagating on top of the bed of nails. The phase matching at this boundary ensures that the wave has to be totally reflected. Therefore, by using this bed of nails it is possible to replace the vertical PMC walls by the structure shown in Fig. 6. Hence, the dispersion equations (8)-(11) of the bed of nails can be used for designing the operating band of a complete RGW coupler.

### B. DISPERSION DIAGRAM OF THE COMPLETE RGW

In order to realize the complete ridge gap waveguide, a metal ridge with width is inserted into the bed of nails as shown in Fig. 8a. Considering the example in Sec. III, the common

section width can be chosen as  $w = 13$  mm in order to guarantee both the fundamental (quasi TEM mode) and the first higher order modes are excited over the bandwidth. Within such structure, quasi TEM mode and the first higher order mode are propagating along  $z$ -direction with phase  $e^{-jk_z z}$ .

In order to satisfy the boundary conditions of this structure, where the cells act as PMC boundary at both ridge sides, one can write the expression for the electric field component on the ridge as follows,

$$E_y = \sum_{m=0,2,4}^{\infty} E_m \cos(k_{xm}x) e^{-jk_z z} + \sum_{m=1,3,5}^{\infty} E_m \sin(k_{xm}x) e^{-jk_z z} \quad (12)$$

where  $x = 0$  is taken at the center of the ridge. By deriving the remaining field equations and applying the continuity of the fields along the edge of the walls ( $x = \pm w/2$ ), the dispersion diagram of the quasi TEM mode and the first higher order mode can be stated, respectively, as follows [12], [14]:

$$\sqrt{k^2 - k_z^2} \tan\left(\sqrt{k^2 - k_z^2} \frac{w}{2}\right) (k^2 - \tilde{k}_y^2) + \frac{k_z^2 \tilde{k}_y^2 - k^2 \sqrt{k_z^2 - k^2 + \tilde{k}_y^2} \sqrt{k_z^2 - k^2 + \tilde{k}_y^2}}{\sqrt{k_z^2 - k^2 + \tilde{k}_y^2}} = 0 \quad (13)$$

$$\sqrt{k^2 - k_z^2} \cot\left(\sqrt{k^2 - k_z^2} \frac{w}{2}\right) (k^2 - \tilde{k}_y^2) - \frac{k_z^2 \tilde{k}_y^2 - k^2 \sqrt{k_z^2 - k^2 + \tilde{k}_y^2} \sqrt{k_z^2 - k^2 + \tilde{k}_y^2}}{\sqrt{k_z^2 - k^2 + \tilde{k}_y^2}} = 0 \quad (14)$$

where  $\tilde{k}_y = k_y$  for TM solution in (9),  $\tilde{k}_y = k_y$  for TE solution in (8).

A Matlab code is used to solve the above transcendental equations, from which the dispersion curves of the quasi TEM mode and the first higher order mode are obtained and shown in Fig. 8b. From this figure, it is clear that there are only two modes propagating within the 10 to 17 GHz band. Those modes are the quasi TEM mode and the first higher order mode. There is a good agreement between the analytical solution and the full wave solution that comes from HFSS eigenmode mode solver.

To verify the relation between the Hybrid PEC/PMC waveguide and the real one realized by the bed of nails, the results of Fig 4c are added to those of Fig. 8b and presented in Fig. 9. From the comparison in Fig. 9, it can be observed that the cut-off frequency of the higher order mode depends on the width of the ridge. From Fig 9, it can be depicted also that there is an agreement in the behavior among the theoretical, simulated results and the hybrid PEC/PMC waveguide model. However, there is a slight difference in the cut off frequency of the odd mode of the RGW and the hybrid PEC/PMC waveguide model.

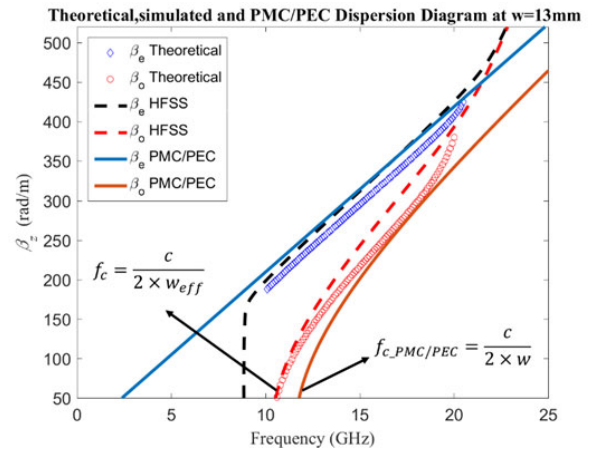


**FIGURE 9.** Dispersion curves for the common waveguide of RGW coupler obtained from, hybrid PEC/PMC theoretical model (solid lines), theoretical analysis of RGW coupler (circles and diamonds) and simulation results of RGW coupler (dashed lines) where  $w = 13$  mm.

This observation conveys an important information about how to use the design rules shown in Sec. III for RGW coupler without causing any shift in the coupler bandwidth.

The interpretation of this deviation is that the electrical width of any RGW is slightly different from PEC/PMC waveguide. Thus, it is very important to find the relation between the effective width of the RGW and the hybrid PEC/PMC waveguide width. This effective width of this structure can be deduced from the cutoff frequency obtained from the dispersion diagram where,

$$w_{eff} = \frac{c}{2f_c} \approx 1.1 \times w \quad (15)$$

In Fig.9, the cut-off frequency of the RGW is 10.57 GHz, therefore its effective width  $w_{eff}$  is 14.2 mm which is about 10% wider than the real width of the ridge. If this value of the effective width is used as the width of the hybrid PEC/PMC waveguide, the obtained dispersion diagram will be exactly the dispersion diagram required for designing the RGW coupler.

As a validation for the previously-discussed concept, the dispersion curves of the RGW coupler and the hybrid PEC/PMC waveguide coupler that has a width equal to the calculated effective width of the RGW are shown in Fig. 10a. From this comparison, it is very clear that there is an excellent agreement between theoretical and simulation results. This directly means that the width of any RGW is not the physical width, but it is an effective width that should be obtained from its dispersion. Consequently, the required coupling length based on the obtained effective width is demonstrated in Fig. 10b based solely on the PEC/PMC waveguide dispersion of Fig. 2a or Fig. 4c.

As a conclusion, the design of any RGW-based microwave component is related to the effective width of the RGW not the physical width dimension. The relation in (15) is of course specific to this example. However, it is not expected to deviate much in other examples. Therefore, it is the task of

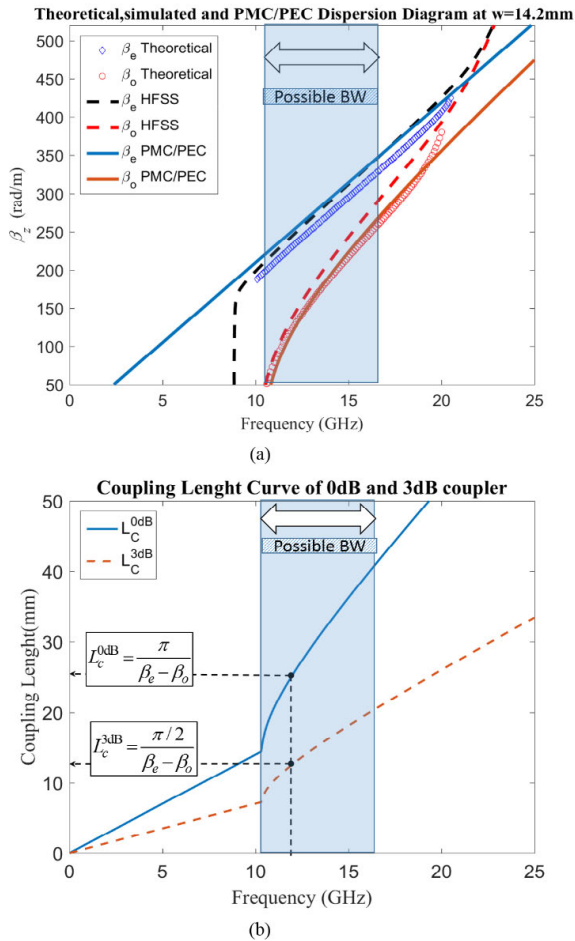


**FIGURE 10.** (a) Dispersion curves of the RGW coupler and the hybrid PEC/PMC waveguide with width equal to the effective width, (b) coupling length versus frequency for both of a 0dB and a 3dB couplers.

the designer to recheck the performance of the final product if the dimensions are initially selected based on (15).

**C. EXCITATION BASED ON PEC/PMC CIRCULAR BEND**

Physically, it is impossible to design the ports beside each other as in the hybrid PEC/PMC waveguide. An enough space should be kept for at least one or two rows of pins to operate as a PMC. Because of that, it is selected to deliver the signal through circular bends. The amplitude and phase responses of a circulating RGW is calculated analytically in this section. The introduced phase shift by circulating RGW has not been previously studied in details. In many applications, the phase shifter is considered as a crucial element especially in beam-forming networks. As usual, a phase shift or delay line is designed in bent shapes rather than in straight lines. Therefore, it is very important to study the phase response in such a curve-shaped RGW. The hybrid PEC/PMC waveguide is used to calculate the phase response of circulating bends at the input and output ports of the RGW coupler. This is to facilitate and simplify the theoretical analysis which would be rather complicated if the RGW is analyzed directly in its complete form.

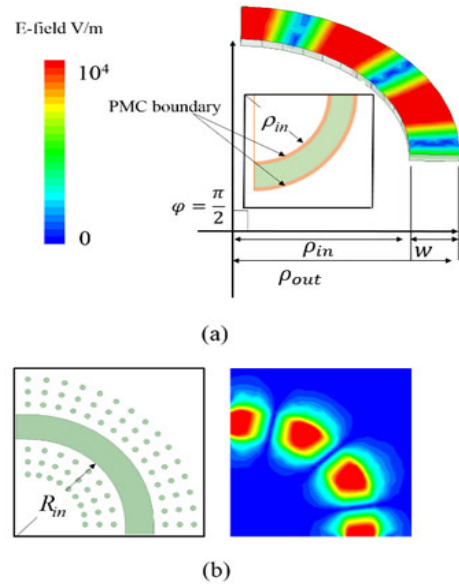


**FIGURE 11.** Circulating hybrid PEC/PMC and Realistic waveguide bends with the corresponding field distributions.

In Fig. 11, a circulating bend hybrid PEC/PMC waveguide equivalent to the curved RGW is presented. The operation of the circulating bend hybrid PEC/PMC waveguide is introduced in this section and the relation between this hybrid PEC/PMC waveguide and the realistic ridge gap circulating bend waveguide is explained.

The proposed geometry of the input and the output ports is a circulating waveguide bend with cross section  $w \times h$ , inner radius  $\rho_{in}$  and outer radius  $\rho_{out} = \rho_{in} + w$ . The same problem was presented earlier for the conventional metallic rectangular waveguide [21]. Therefore, by using the same methodology and changing the boundaries according to the proposed design, the resultant operation can be deduced. The wave function in circular bend waveguide can be written as [20]:

$$\psi = [AJ_n(k\rho) + BN_n(k\rho)] \exp(-jn\varphi) \quad (16)$$

where  $J_n(k\rho)$  is the Bessel function of the first kind of order  $n$ ,  $N_n(k\rho)$  is the Bessel function of the second kind of order  $n$ , and  $\rho, \varphi$  are the cylindrical coordinates and  $A$  is an arbitrary constant. The constant  $n$  represents the propagation constant in  $\varphi$ -direction. This is the unknown which needs to be calculated. The wave function  $\psi$ , in (17) is used to derive the full expressions for the electric and magnetic fields. However, this can be done for two types of possible solutions, namely the  $TM^z$  and  $TE^z$ . The boundary conditions in the problem at hand dictates that the solution of interest is the  $TM^z$ . The general solution for  $TM^z$  modes must satisfy [21]:

$$J'_n(k_\rho \rho_{in}) N'_n(k_\rho \rho_{out}) - J'_n(k_\rho \rho_{out}) N'_n(k_\rho \rho_{in}) = 0 \quad (17)$$

where  $k_\rho = k$ . Equation (18) is solved numerically for the unknown,  $n$ . For example, consider the circulating waveguide designed in Section III to be of inner radius and outer radius



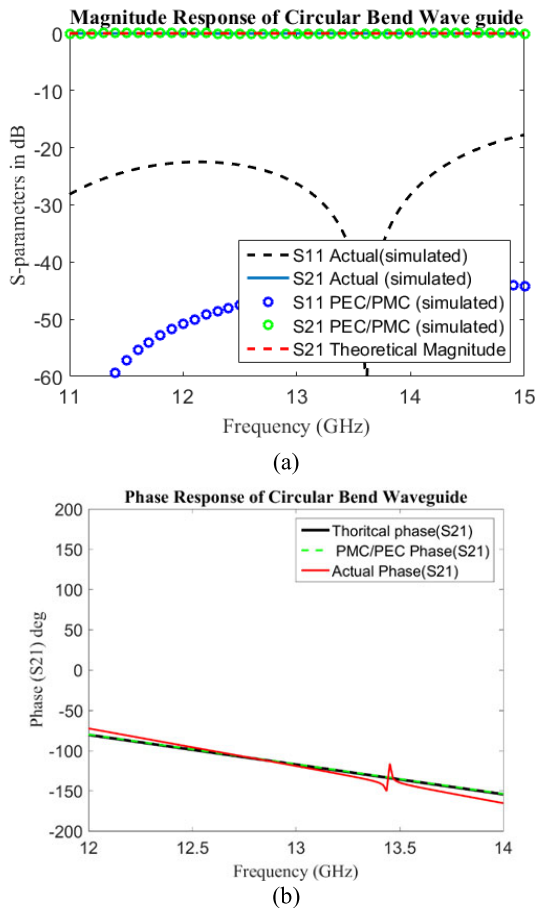


**FIGURE 12.** Comparison among the theoretical, Realistic and hybrid PEC/PMC phase and magnitude response of circular bend waveguide: (a) Magnitude response, (b) phase response.

$\rho_{out} = 22 \text{ mm}$  and  $\varphi = \pi/2$  as shown in Fig. 11. This radius is chosen to minimize the reflections and maximize the transmission through the bend.

A Comparison is illustrated in Fig. 12 among the hybrid simulated PEC/PMC waveguide bend, theoretical analysis and the simulated realistic waveguide bend. The magnitude and phase responses are shown in Figs. 12(a) and 12(b), respectively. The magnitude response of such waveguide is perfect, but the more significant is the phase response which is critical if the coupler is to be included in beamforming networks such as Butler matrix. From Figs. 12a and 12b, it can be depicted that there is an agreement in the behavior of magnitude and phase responses among the theoretical, realistic simulated results and the hybrid PEC/PMC waveguide model from 12.5-13.5 GHz. However, there is a slight difference in phase at frequencies far from the center frequency. The interpretation of this deviation is that the bed of nails surrounding the ridge act as PMC just around the 13GHz.

**D. THE FULL RGW COUPLER**

In this section, PMC boundaries are replaced by the periodic unit cells. The unit cell dimensions are the same as presented

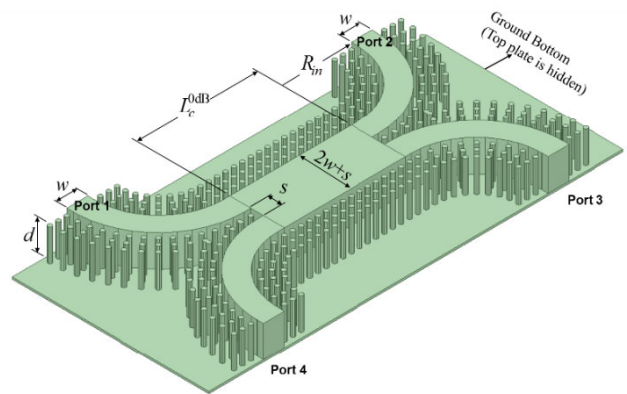


**FIGURE 13.** The physical structure of the RGW 0dB coupler.

in Sec. IV-A in order to operate over an approximate bandwidth of (10-17) GHz. The complete structure of a 0dB RGW coupler is presented in Fig. 13 where the top metal plate is hidden to show the inside structure. The coupling length  $L_c$  is obtained from the graph shown in Fig. 10(b) and (6) based on what is obtained from the hybrid PEC/PMC waveguide coupler.

By using the obtained effective width, the required coupling length becomes 29 mm. For a physical connection to the input and output ports, they are designed based on circulating bends as explained in Sec. IV-C.

The field distribution and the scattering parameters of the designed RGW coupler are shown in Figs. 14a and 14b, respectively. From those figures, it can be observed that the proposed design methodology resulted in an excellent operation of the RGW coupler exactly at the selected design frequency where full coupling occurs.

**E. FREQUENCY-TUNABLE RGW COUPLER**

One of the most important features that may exist in a microwave component is the tuning capability. The tunability of the RGW is not widely-reported in the literature. For example, in [23], an electrically-tunable planar groove gap waveguide resonant cavity is presented. In the referred example, the tunability is achieved by using a nonlinear varactor element.

In this section, it is shown that the frequency tuning could be achieved easily without the need of using nonlinear elements. This could be achieved by just slightly moving the upper conducting plate of the RGW which controls the height  $h$  of the RGW. The effect of changing the height  $h$  is shown in Fig. 15. It could be clearly observed from this figure that the propagation constant of the odd mode has different values for different heights at each single frequency. The difference in the propagation constant reaches to  $45,7 \text{ rad/m}$  with only 2.5 mm change in the height.

On the other hand, the propagation constant of the even mode is almost independent on the height. Therefore, the coupling length obtained from equation (6) may have different values for different heights as shown in Fig. 16. This means

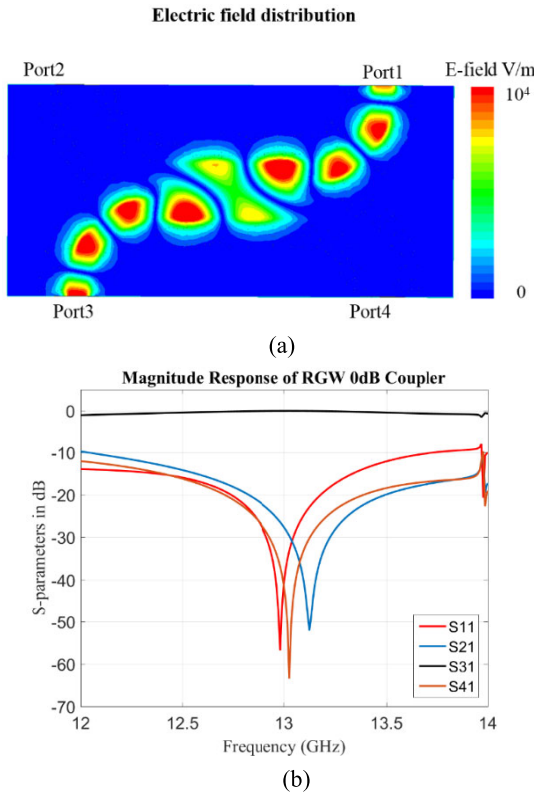


FIGURE 14. Full wave simulation for the 0dB RGW coupler at 13 GHz, (a) electric field distribution and (b) magnitude of S-parameters.

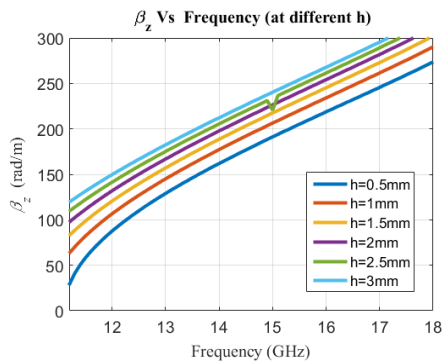


FIGURE 15. The behavior of odd mode versus the air gap height.

that controlling the height of the upper conducting plate may tune the coupler center frequency as shown in Fig. 17. The tunability mechanism is feasible, especially the upper conducting plate of the RGW is not attached to the lower plate.

V. A POSSIBLE SETUP FOR PROTOTYPING THE PROPOSED RGW COUPLER

A. MICROSTRIP TO RGW TRANSITION

In order to physically excite and measure the performance of the proposed structure by a Vector Network Analyzer (VNA), four microstrip transitions to RGW are needed. Those transitions should cover the whole bandwidth of our design with

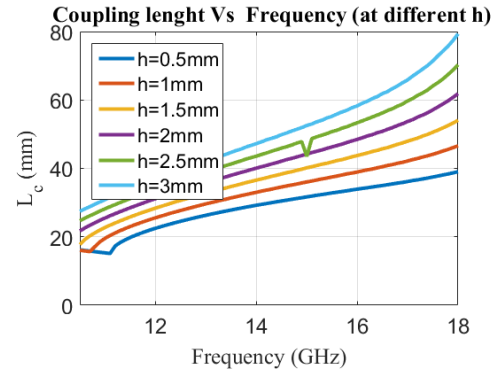


FIGURE 16. The coupling length versus the air gap height.

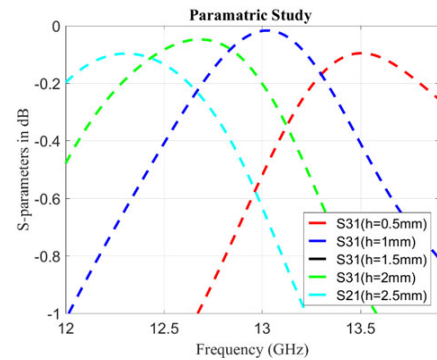


FIGURE 17. Full wave simulation for the 0dB RGW coupler at 13 GHz: Magnitude S-parameters (S31 and S21) versus the air gap height.

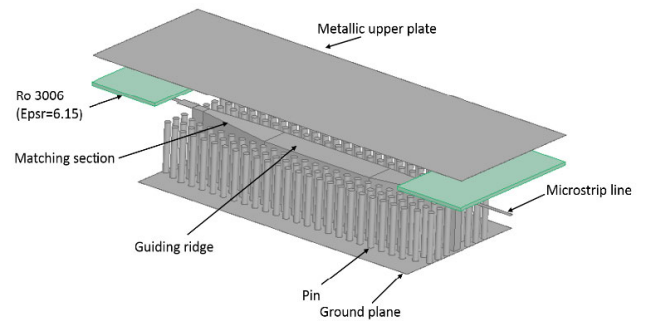


FIGURE 18. Microstrip to metallic ridge gap waveguide transition.

less than -15 dB in back to back configuration. Several models of transition are presented in [24], [26]. Based on previous references, a transition from microstrip waveguide to metallic RGW is designed and tested with the whole 0dB coupler structure. The microstrip transition is shown in Fig.18. The design is very simple, which the transition of microstrip is printed over Ro-3006 dielectric substrate with  $\epsilon_r = 6.15$ . In this transition, the microstrip line is located on the ridgeline of the RGW. Therefore, the microstrip mode will transform gradually to the air-filled ridge gap waveguide mode. Due to the standers of the substrate height of the microstrip line, the size of the air gap should be changed gradually to be equal to the substrate height. The changing of air gap size

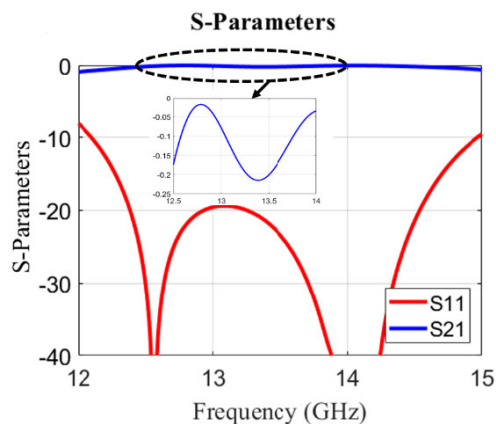
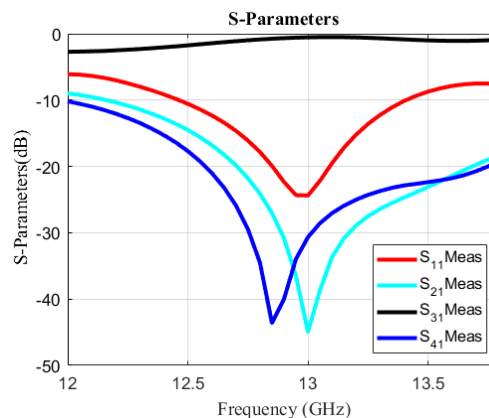
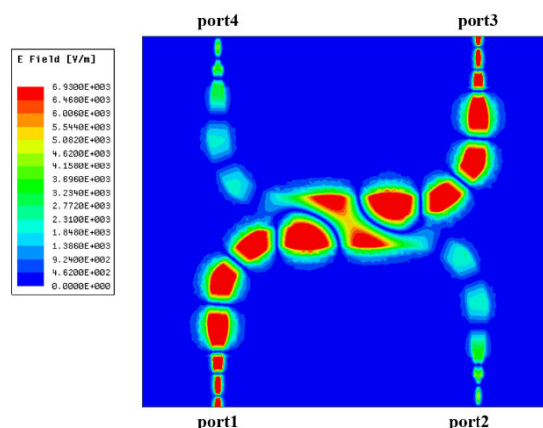


FIGURE 19. Simulated results microstrip to metallic ridge gap waveguide transition.



(a)



(b)

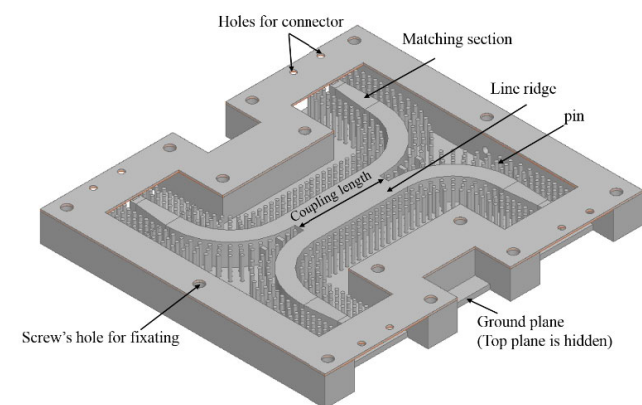


FIGURE 20. The whole setup model of 0dB coupler include the microstrip transition without top plate.

is achieved by tapering the height of the matching section. Two microstrip transitions to RGW are used in a back-to-back design is illustrated in Fig. 18. The result of the back-to-back transition is shown in Fig. 19. It can be noted that the S11 is below  $-20$  dB from 12.5 to 14.5 GHz, and S21 is about 0.2 dB.

**B. WHOLE SETUP MODEL OF 0DB COUPLER INCLUDE THE MICROSTRIP TRANSITION.**

The whole structure of 0dB coupler with the designed transitions is solved numerically before the fabrication stage. Also, the main body proposed structure is passive and made completely of air-filled metallic cavities, and it is expected that the measurement results will agree with the simulation results. Fig. 20 shows the complete model setup of the 0dB coupler, where the top metal plate is hidden to show the internal details of the structure.

The scattering parameters and field distribution of the designed RGW coupler are shown in Figs. 21a and b, respectively. From this figure, it can be concluded that the proposed design methodology resulted in an excellent operation of the RGW coupler. Where a full coupling occurs exactly at the selected design frequency

FIGURE 21. Simulated scattering parameters and Electric field distribution of the whole setup model of 0dB coupler include the microstrip transition. (a) Scattering parameters, (b) Electric field distribution.

**C. FABRICATION AND EXPERIMENTAL RESULTS**

To verify the proposed design, a prototype of the 0dB coupler is fabricated and measured, as shown in Fig. 22. The main body of the 0dB coupler and the microstrip transition are manufactured separately. Then all parts are gathered by bolts. We use plastic 3D printing technology to build the main structure of the 0dB coupler. The 3D printer utilizes an opaque white SLA plastic that behaves similarly to polycarbonate and has elevated heat resistant. Then, the printed structure is electroplated with 0.02-mm thick copper material. While the PCB technology is used to fabricate the microstrip transition and the top plate. Fig. 22(a) and (b) show the individual parts and the assembled 0dB coupler with the connectors respectively.

The measured and simulated S parameters of the proposed design are illustrated in Fig. 23. From this figure, it can be observed that the measured and simulated results in good agreement. The designed coupler works perfectly at the selected design frequency where full coupling occurs at 13GHz. Moreover, the measured isolation better than 20dB over the whole band. The insertion loss in setups is around 0.7 dB, due to the fabrication tolerance and connectors. However, this affects the configuration



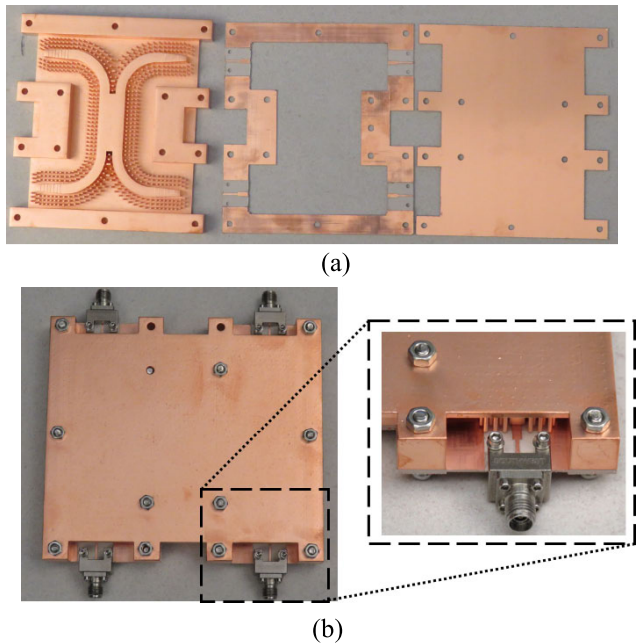


**FIGURE 22.** Pictures of the fabricated individual parts and assembled structure. (a) Individual parts of designed 0dB coupler, (b) Assembled 0dB coupler.

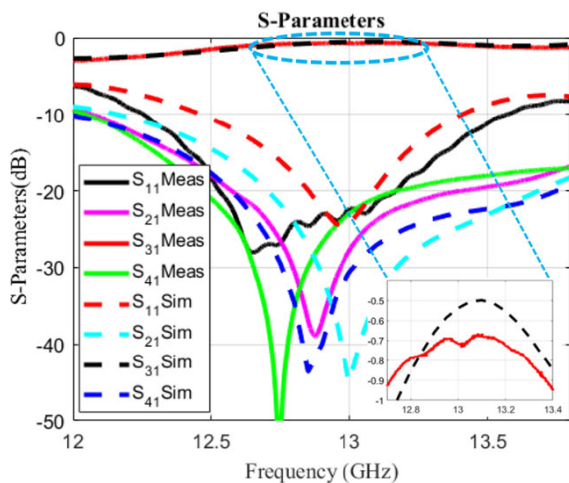


**FIGURE 23.** Measured and simulated scattering parameters of the whole setup model of 0dB coupler include the microstrip transition.

dimensions, which can lead to a small shift and losses in the measurement results. Also, since the design is plated with copper, it can be oxidized over time. Therefore, it might increase the losses.

## VI. CONCLUSION

In this paper, a design methodology is presented for a hybrid junction based on RGW technology. The presented methodology depends on the operation of a hybrid PEC/PMC waveguide. This hybrid waveguide shows a great potential for an accurate estimation for the required dimensions of the RGW coupler to operate at a specific frequency band. It has been deduced from that model that an RGW acts with an effective width that needs to be calculated precisely. The analysis of

the phase response introduced by a circulating RGW bend is introduced. The possibility of tuning the center frequency of a RGW coupler is introduced by moving the upper conducting plate of the RGW. The measurement and simulation results of the complete model setup of the 0dB coupler are compared to each other. The results show acceptable levels compared to each other's and shown that the 0dB coupler works effectively with calculated coupling length from the proposed PEC/PMC model.

## REFERENCES

- [1] W. A. Tyrrell, "Hybrid circuits for microwaves," *Proc. IRE.*, vol. 35, no. 11, pp. 1294–1306, Nov. 1947.
- [2] S. B. Cohn, "The re-entrant cross section and wide-band 3-dB hybrid couplers," *IEEE Trans. Microw. Theory Techn.*, vol. MTT-11, no. 4, pp. 254–258, Jul. 1963.
- [3] B. Sheleg and B. E. Spielman, "Broadband (7–18 GHz) 10 dB overlay coupler for MIC application," *Electron. Lett.*, vol. 11, no. 8, pp. 175–176, Apr. 1975.
- [4] G. H. Zhai, W. Hong, K. Wu, J. X. Chen, P. Chen, J. Wei, and H. J. Tang, "Folded half mode substrate integrated waveguide 3 dB coupler," *IEEE Microw. Wireless Compon. Lett.*, vol. 18, no. 8, pp. 512–514, Aug. 2008.
- [5] A. A. Sakr, W. M. Dyab, and K. Wu, "Theory of polarization-selective coupling and its application to design of planar orthomode transducers," *IEEE Trans. Antennas Propag.*, vol. 66, no. 2, pp. 749–762, Feb. 2018.
- [6] A. A. Sakr, W. M. Dyab, and K. Wu, "Design methodologies of compact orthomode transducers based on mechanism of polarization selectivity," *IEEE Trans. Microw. Theory Techn.*, vol. 66, no. 3, pp. 1279–1290, Mar. 2018.
- [7] S. I. Shams and A. A. Kishk, "Design of 3-dB hybrid coupler based on RGW technology," *IEEE Trans. Microw. Theory Techn.*, vol. 65, no. 10, pp. 3849–3855, Oct. 2017.
- [8] M. M. M. Ali, S. I. Shams, and A. Sebak, "Ultra-wideband printed ridge gap waveguide hybrid directional coupler for millimetre wave applications," *IET Microw., Antennas Propag.*, vol. 13, no. 8, pp. 1181–1187, Jul. 2019.
- [9] M. Farahani, M. Akbari, M. Nedil, T. A. Denidni, and A. R. Sebak, "A novel low-loss millimeter-wave 3-dB 90° ridge-gap coupler using large aperture progressive phase compensation," *IEEE Access*, vol. 5, pp. 9610–9618, 2017.
- [10] F. Boccardi, R. W. Heath, Jr., A. Lozano, T. L. Marzetta, and P. Popovski, "Five disruptive technology directions for 5G," *IEEE Commun. Mag.*, vol. 52, no. 2, pp. 74–80, Feb. 2014.
- [11] A. Vosoogh, P. S. Kildal, and V. Vassilev, "Wideband and high-gain corporate-fed gap waveguide slot array antenna with ETSI class II radiation pattern in V-band," *IEEE Trans. Antennas Propag.*, vol. 65, no. 4, pp. 1823–1831, Apr. 2017.
- [12] A. Vosoogh and P.-S. Kildal, "Corporate-fed planar 60-GHz slot array made of three unconnected metal layers using AMC pin surface for the gap waveguide," *IEEE Antenna Wireless Propag. Lett.*, vol. 15, pp. 1935–1938, Dec. 2015.
- [13] D. Zarifi, A. Farahbakhsh, A. U. Zaman, and P. S. Kildal, "Design and fabrication of a high-gain 60-GHz corrugated slot antenna array with ridge gap waveguide distribution layer," *IEEE Trans. Antennas Propag.*, vol. 64, no. 7, pp. 2905–2913, Jul. 2016.
- [14] A. Polemi, S. Maci, and P.-S. Kildal, "Dispersion characteristics of a metamaterial-based parallel-plate ridge gap waveguide realized by bed of nails," *IEEE Trans. Antennas Propag.*, vol. 59, no. 3, pp. 904–913, Mar. 2011.
- [15] P.-S. Kildal, E. Alfonso, A. Valero-Nogueira, and E. Rajo-Iglesias, "Local metamaterial-based waveguides in gaps between parallel metal plates," *IEEE Antennas Wireless Propag. Lett.*, vol. 8, no. 4, pp. 84–87, Apr. 2009.
- [16] A. Polemi and S. Maci, "Closed form expressions for the modal dispersion equations and for the characteristic impedance of a metamaterial-based gap waveguide," *IET Microw., Antennas Propag.*, vol. 4, no. 8, pp. 1073–1080, Aug. 2010.
- [17] A. T. Hassan, M. A. Moharram, and A. A. Kishk, "Empirical analysis formulae of microstrip ridge gap waveguide," in *Proc. IEEE Int. Symp. Antennas Propag., USNC/URSI Nat. Radio Sci. Meeting*, Boston, MA, USA, Jul. 2018, pp. 423–424.



- [18] M. M. M. Ali, S. I. Shams, and A.-R. Sebak, "Printed ridge gap waveguide 3-dB coupler: Analysis and design procedure," *IEEE Access*, vol. 6, pp. 8501–8509, 2017.
- [19] A. Beltayib, I. Afifi, and A.-R. Sebak, " $4 \times 4$ -element cavity slot antenna differentially-fed by odd mode ridge gap waveguide," *IEEE Access*, vol. 7, pp. 48185–48195, 2019.
- [20] H. J. Riblet, "The short-slot hybrid junction," *Proc. IRE*, vol. 40, no. 2, pp. 180–184, Feb. 1952.
- [21] R. F. Harrington, *Time-Harmonic Electromagnetic Fields*. Hoboken, NJ, USA: Wiley, 2001.
- [22] R. Mongia, I. J. Bahl, and P. Bhartia, *RF and Microwave Coupled-line Circuits*. Norwood, MA, USA: Artech House, 2007.
- [23] T. Oyedokun, R. Geschke, and T. Stander, "A tunable Ka-band planar groove gap waveguide resonant cavity," in *Proc. IEEE Radio Antenna Days Indian Ocean (RADIO)*, Sep. 2017, pp. 1–2.
- [24] A. A. Brazález, A. U. Zaman, and P.-S. Kildal, "Investigation of a microstrip-to-ridge gap waveguide transition by electromagnetic coupling," in *Proc. IEEE Int. Symp. Antennas Propag.*, Chicago, IL, USA, Jul. 2012, pp. 1–2.
- [25] A. U. Zaman, T. Vukusic, M. Alexanderson, and P.-S. Kildal, "Design of a simple transition from microstrip to ridge gap waveguide suited for MMIC and antenna integration," *IEEE Antennas Wireless Propag. Lett.*, vol. 12, pp. 1558–1561, 2013.
- [26] A. Brazález, J. Flygare, J. Yang, V. Vassilev, M. Baquero-Escudero, and P. Kildal, "Design of  $F$ -band transition from microstrip to ridge gap waveguide including Monte Carlo assembly tolerance analysis," *IEEE Trans. Microw. Theory Techn.*, vol. 64, no. 4, pp. 1245–1254, Apr. 2016.



**ABDEL-RAZIK SEBAK** (LF'10) received the B.Sc. degree (Hons.) in electrical engineering from Cairo University, Cairo, Egypt, in 1976, the B.Sc. degree in applied mathematics from Ain Shams University, Cairo, in 1978, and the M.Eng. and Ph.D. degrees in electrical engineering from the University of Manitoba, Winnipeg, MB, Canada, in 1982 and 1984, respectively. From 1984 to 1986, he was with Canadian Marconi Company, involved in the design of microstrip phased array antennas. From 1987 to 2002, he was a Professor with the Department of Electronics and Communication Engineering, University of Manitoba. He is currently a Professor with the Department of Electrical and Computer Engineering, Concordia University, Montreal, QC, Canada. His research interests include phased array antennas, millimeter-wave antennas and imaging, computational electromagnetics, and interaction of EM waves with engineered materials and bio electromagnetics. He is also a member of the Canadian National Committee of International Union of Radio Science Commission B. He was a recipient of the 2000 and 1992 University of Manitoba Merit Award for outstanding Teaching and Research, the 1994 Rh Award for Outstanding Contributions to Scholarship and Research, and the 1996 Faculty of Engineering Superior. He has served as the Chair for the IEEE Canada Awards and Recognition Committee, from 2002 to 2004, and as a Technical Program Chair of the 2002 IEEE CCECE Conference and the 2006 URSIANTEM Symposium. He is also a Technical Program CoChair of the 2015 IEEE ICUWB Conference.

...



**ABDULADEEM BELTAYIB** received the B.Sc. degree in electronics and communications engineering from the College of Electronic Technology, Baniwaleed, Libya, in 2003, and the M.Sc. degree in electrical and computer engineering from the Libyan Academy, Libya, in 2007. He is currently pursuing the Ph.D. degree in electrical and computer engineering, Concordia University, Montreal, QC, Canada. From 2008 to 2013, he was a Lecturer with the Communication Department of the Faculty of Engineering, Baniwaleed High Institution Electronics Technology. He was a Teaching Assistant with the Department of communication Engineering, Libya. His current research interests include analysis and antenna design, high gain millimeter-wave antennas, and ridge gap waveguide and metamaterial.